Journal of Solid State Chemistry 184 (2011) 1530–1539

Contents lists available at ScienceDirect

Journal of Solid State Chemistry

journal homepage: www.elsevier.com/locate/jssc

Structural and magnetic properties of nanoclusters in GaMnAs granular layers

K. Lawniczak-Jablonska [a,*], J. Bak-Misiuk [a], E. Dynowska [a], P. Romanowski [a], J.Z. Domagala [a], J. Libera [a], A. Wolska [a], M.T. Klepka [a], P. Dluzewski [a], J. Sadowski [a,b], A. Barcz [a], D. Wasik [c], A. Twardowski [c], A. Kwiatkowski [c]

[a] Institute of Physics PAS, al. Lotnikow 32/46, PL-02668 Warsaw, Poland
[b] MAX-Lab, Lund University, P.O. Box. 118, S-22100 Lund, Sweden
[c] Institute of Experimental Physics, Faculty of Physics, University of Warsaw, ul. Hoza 69, PL-00681 Warsaw, Poland

ARTICLE INFO

Article history:
Received 10 February 2011
Received in revised form
14 April 2011
Accepted 18 April 2011
Available online 23 April 2011

Keywords:
GaMnAs
Semiconductors
Nanoclusters
Spintronics
Ferromagnetism

ABSTRACT

Structural and magnetic properties of GaAs thin films with embedded nanoclusters were investigated as a function of the annealing temperature and Mn content. Surprisingly, the presence of two kinds of nanoclusters with different structure was detected in most of the samples independently of the thermal processing or Mn content. This proved that the presence of a given type of clusters cannot be assumed a priori as is reported in many papers. The fraction of Mn atoms in each kind of cluster was estimated from the extended X-ray absorption fine structure analysis. This analysis ruled out the possibility of the existence of nanoclusters containing a hypothetic MnAs cubic compound—only (Ga,Mn)As cubic and hexagonal MnAs clusters were detected. Moreover the bimodal distribution of Mn magnetic moments was found, which scales with the estimated fraction of Mn atoms in the cubic and hexagonal clusters.
© 2011 Elsevier Inc. All rights reserved.

1. Introduction

Magnetic semiconductors with carrier-induced ferromagnetism have received a lot of interest, since they hold out prospects for using electron spins in electronic devices. $Ga_{1-x}Mn_xAs$ is one of the diluted magnetic semiconductor materials (DMS), which has been the most extensively studied after its discovery in 1996 by Ohno et al. [1]. It has attracted a great deal of attention both as an object of basic studies of DMS systems [2–4] and as a versatile material suitable for testing prototype spintronic devices [5–8]. The low solubility limit of Mn in GaAs (less than 0.1%) has been overcome by use of low temperature molecular beam epitaxial (MBE) growth, for preparation of monocrystalline GaMnAs layers. MBE is a highly nonequilibrium crystal growth method; moreover, the use of extremely low (as for GaAs) growth temperatures, in the range of 170–250 °C, allows the creation of GaMnAs ternary alloy with nominal Mn content much higher than the solubility limit [9,10]. Mn located at Ga sites in GaAs host is an acceptor and gives a very large concentration of holes (in the range of 10^{20}–10^{21} cm^{-3}) with Mn content in the range of a few percent. However, due to the low crystallization temperature, GaMnAs layer contains point defects retaining donor character and partially compensating the Mn_{Ga} acceptors. The most important defects of this kind are As antisites (As_{Ga}) and Mn interstitials (Mn_I). In order to optimize the properties of GaMnAs such as conductivity and ferromagnetic phase transition temperature (T_c), it is necessary to minimize the concentration of these compensating defects. The concentration of As_{Ga} can be minimized by a choice of suitable conditions for low temperature MBE growth [10]. On the other hand, the concentration of Mn_I defects can be highly reduced by the use of low temperature (170–250 °C) post-growth annealing procedures [11–13].

Low temperature (*LT*) annealing of thin GaMnAs epitaxial layers at temperatures up to 250 °C causes a decrease of the layer lattice parameter due to removal of the Mn interstials, which form double donors [14]. A reduction of Mn interstitials leads to enhanced carrier concentration and Curie temperature. The present T_c record in the diluted $Ga_{1-x}Mn_xAs$ material is about 190 K [15], which is remarkably high for a DMS material but still too low for application purposes.

On the other hand, it has been demonstrated that, as an effect of high temperatures (*HT*) annealing at 400–700 °C of the GaMnAs layers [16–21] or the Mn-implanted GaAs crystals [22] ferromagnetic MnAs precipitates are fairly easily produced, yielding multi-phase materials. The granular GaAs:Mn material exhibits a ferromagnetic/superparamagnetic behavior at room temperature, depending on the cluster size [21]. Such composite systems are currently thoroughly investigated [23–27]. In many papers it is assumed without experimental proof that after annealing at temperature close to 600 °C only hexagonal clusters are formed

* Corresponding author.
E-mail address: jablo@ifpan.edu.pl (K. Lawniczak-Jablonska).

0022-4596/$ - see front matter © 2011 Elsevier Inc. All rights reserved.
doi:10.1016/j.jssc.2011.04.033

(e.g. [28]), and they are responsible for the magnetic properties that are not true as was recently reported [29] and will be shown below. In this context we believe that it is very important to perform a systematic and comprehensive study of the properties of the GaAs:Mn granular system in a function of Mn content and annealing conditions and correlate the type of created clusters with magnetic properties.

The X-ray diffraction (XRD) and transmission electron microscopy (TEM) methods were applied to get full information about the structure and dimensions distribution of clusters and the related values of strains in GaAs:Mn granular layers. Neither of these methods provides knowledge about the fraction of Mn being bonded in each of the detected kind of nanoclusters. Therefore, X-ray absorption spectroscopy (XAS) was also applied. To control the Mn content and depth profile after annealing, secondary ion mass spectroscopy (SIMS) was used. Finally, the magnetic properties of samples were measured and related to structural properties.

2. Experimental

$Ga_{1-x}Mn_xAs$ layers with nominal Mn contents $x=0.015$, 0.06, 0.07 and 0.08 were grown by MBE on the (001)-oriented GaAs substrates at a temperature of 230 °C. The nominal thickness of the layers was 0.8 μm. After deposition each sample was cut into three pieces: one of them was left untreated, and the remaining were reintroduced into the MBE growth chamber and annealed under As_2 flux for 30 min at $T=500$ °C and at $T=600$ °C, respectively.

To estimate the real Mn contents in $Ga_{1-x}Mn_xAs$ layers and to check the influence of annealing on the distribution of Mn atoms inside them, SIMS measurements using the CAMECA IMS6F microanalyzer were carried out. These measurements were performed with an oxygen (O_2^+) primary beam, with the current kept at 600 nA. The size of the eroded crater was about 150 μm × 150 μm and the secondary ions were collected from the central region of 60 μm in diameter. The Mn content was derived from the intensity of the Mn^+ species and the matrix signal, As^+, was taken as a reference. Mn implanted GaAs was used as a calibration standard. The accuracy of the Mn content determination in the SIMS method is ~5%. The thickness of the examined layers was measured by an Alpha-Step Profiler.

The X-ray measurements were performed using a high resolution Philips material research diffractometer (MRD) in double and triple crystal configuration, equipped with a standard laboratory source of Cu$K\alpha_1$ radiation. Moreover, the measurements with the use of monochromatic synchrotron radiation ($\lambda=1.54056$ Å) at the W1 beamline at DESY-HASYLAB were also performed.

The out-of-plane ($a_\perp$) and in-plane ($a_{||}$) lattice parameters were calculated from $2\theta/\omega$ in the vicinity of the 004 symmetrical and 224 asymmetrical reflections. The relaxed lattice parameter (a_{rel}) and the in-plane strain (ε) for each layer were calculated according to the formulas:

$$a_{rel}=\frac{a_\perp+\nu a_{||}}{1+\nu}, \quad (1)$$

where

$\nu=2\frac{c_{12}}{c_{11}}$ –Poisson's ratio for cubic crystals

$$\varepsilon=\frac{a_{||}-a_{rel}}{a_{rel}} \quad (2)$$

The XRD determination of the lattice parameters of hexagonal MnAs nanoclusters was possible using synchrotron radiation. The orientation of the MnAs nanoclusters embedded in GaAs matrix is well-defined [17]: (00.1) planes of MnAs are parallel to {111} GaAs planes, the (01.0) MnAs directions are parallel to $\langle 1\bar{1}2\rangle$ GaAs directions, and the $\langle 11.0\rangle$ MnAs directions are parallel to $\langle 1\bar{1}0\rangle$ or $\langle 11.0\rangle$ GaAs directions. Therefore, the lattice parameters of hexagonal MnAs were calculated from 02.2 and 03.0 reflections that were detected by the ω scan in the vicinity of symmetrical 004 GaAs reflection, and from the $2\theta/\omega$ scan around the asymmetrical 224 GaAs reflection.

TEM studies were carried out using a JEOL 2000EX instrument operating at 200 kV accelerating voltage. The cross-sectional specimens were mechanically polished, dimpled and finally milled with Ar^+ ions beams at 2 kV and 8° inclined to the sample surface. The histograms of nanocluster sizes were obtained from high-resolution images obtained in the $\langle 011\rangle$ projection.

XAS measurements were performed at liquid nitrogen temperature, at the A1 experimental station in DESY-HASYLAB using a double crystal Si (111) monochromator. The Mn K-edge spectra were registered using a seven-element fluorescence Si detector. To reduce the error introduced by the diffraction peaks, which are present in the well-oriented crystalline samples for each sample, several spectra were collected at slightly different angles around 45°. The spectra were averaged and then analyzed.

Magnetization measurements were performed using superconducting quantum interference device (SQUID) magnetometer as a function of temperature (5–325 K) at constant magnetic fields. Magnetic field was applied in-plane of the sample surface. Magnetization data were corrected for the diamagnetic contribution of GaAs substrate.

3. Results and discussion

3.1. Secondary ion mass spectroscopy studies

The concentration of Mn and the thickness of the $Ga_{1-x}Mn_xAs$ layers found from SIMS measurements in the as-grown samples are presented in Fig. 1. The concentration of Mn and thickness of the grown layers differ from nominal values. The smallest content of Mn was $x=0.025$ and the highest $x=0.063$. Some tendency of the Mn accumulation at the interface with the GaAs substrate was observed. Therefore, the relation of the nominal contents $x=0.015$, 0.06, 0.07 and 0.08 to the SIMS values is $x=0.025$, 0.04, 0.05 and 0.063, respectively. In further discussion we will use the

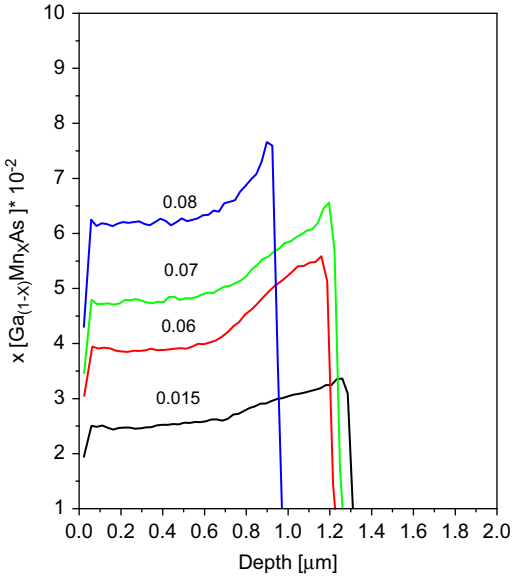

Fig. 1. The Mn concentration x in-depth profiles and layer thickness resulted from SIMS study of the investigated samples. The nominal concentration is given above the curve.

concentration values as estimated by SIMS. The concentration of Mn in all of the examined samples did not change significantly during the annealing. Results of the SIMS measurements for the annealed sample $x=0.04$ are shown in Fig. 2 as an example. During the annealing at 500 and 600 °C Mn atoms did not diffuse significantly to the surface or to the substrate.

3.2. X-ray diffraction studies

The lattice parameters of the investigated layers were calculated from the symmetrical and asymmetrical $2\theta/\omega$ scans performed by the high resolution MRD diffractometer. It was confirmed that all $Ga_{1-x}Mn_xAs$ layers grow on the GaAs substrate pseudomorphically, i.e. the in-plane lattice parameter ($a_{\parallel}$) is equal to that of the GaAs substrate. It was found that the annealing of these layers does not change their in-plane lattice parameter.

The $2\theta/\omega$ scans around 004 GaAs reflection for the as-grown and annealed samples with low ($x=0.025$) and higher Mn concentration ($x=0.05$) are presented in Figs. 3 and 4, respectively. The 004 peaks marked by 1, 2 and 3 originate from layers as-grown, annealed at 500 °C and annealed at 600 °C, respectively.

The position of the 004 peak from the as-grown layer is situated on the left side of the 004 peak from the GaAs substrate, which means that this layer is compressively strained ($a_{\perp layers} > a_{GaAs}$). The relatively large compressive strain of the as-grown layers results from Mn interstitial and As_{Ga} anti-site defects, as well as from Mn in

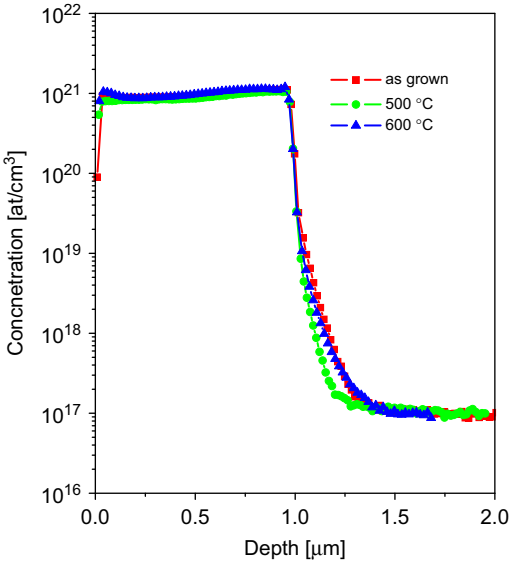

Fig. 2. The concentration of Mn atoms in the sample with $x=0.04$ as-grown and after annealing.

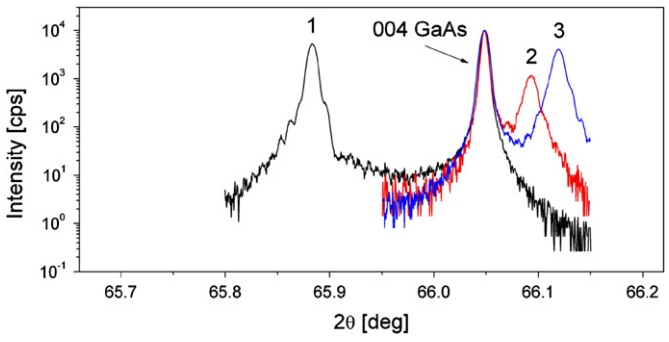

Fig. 3. The $2\theta/\omega$ scans of 004 reflection for GaAs:Mn samples with $x=0.025$: (1)—as-grown, (2)—after annealing at 500 °C and (3)—after annealing at 600 °C.

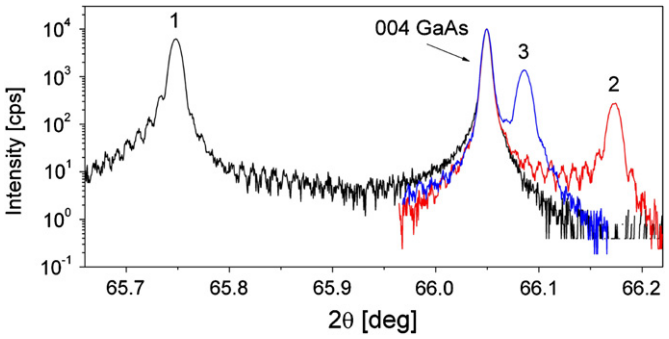

Fig. 4. The $2\theta/\omega$ scans of 004 reflection for GaAs:Mn samples with $x=0.05$: (1)—as-grown, (2)—after annealing at 500 °C and (3)—after annealing at 600 °C.

Ga sites [30–32]. It was also found that for the as-grown layers an increase of Mn content leads to an increase of the $a_{\perp}$ lattice parameter, and, in consequence, to an increase of the strain state (ε). The relaxed lattice parameters (a_{rel}) of these layers are larger than the lattice parameter of GaAs substrate. On the other hand, the positions of 004 peaks originating from the annealed layers are shifted towards higher angles with respect to the position of 004 GaAs peak, which indicates the change of strain state from compressive to tensile ($a_{\perp layers} < a_{GaAs}$). Simultaneously, the relaxed lattice parameters of these layers become smaller than the lattice parameter of GaAs. In the case of lower Mn content ($x=0.025$) the annealing at higher temperature leads to further decrease of the $a_{\perp}$ lattice parameter (Fig. 3), which results in further decrease of a_{rel} and increase of tensile strain. The opposite effect was found for the all layers with higher Mn concentration (e.g. $x=0.05$, Fig. 4)—an increase of annealing temperature to 600 °C leads to an increase of the $a_{\perp}$ lattice parameter and a decrease of tensile strain. The calculated values of the lattice parameters $a_{\perp}$ and a_{rel}, and the in-plane strain state (ε) of the examined layers, are given in Table 1.

The decrease of the lattice parameter of annealed GaMnAs layers is related to the formation of granular GaAs:Mn material consisting of MnAs nanoclusters [16,20,30]. The mechanism of such behavior is not clear, therefore, we made an attempt to explain this effect. In our XRD studies the evidence of hexagonal nanoclusters (in the layers with Mn concentration higher than $x=0.025$) was possible owing to the use of synchrotron radiation. The ω scan recorded around the 004 GaAs reflection (Fig. 5a) allowed the detection of two reflections of 02.2 originating from hexagonal, NiAs-type MnAs nanoclusters (Bragg angles for these reflections are very similar: $\theta=33.30°$ for 02.2 of MnAs bulk and $\theta=33.03°$ for 004 GaAs). The broadening of the 02.2 peaks can be attributed to disorder in the orientations of different MnAs nanoclusters. From the $2\theta/\omega$ scans of 02.2 MnAs reflection (Fig. 5a, inset) and the asymmetrical reflection of 2 2 $\bar{4}$ GaAs (Fig. 5b), the lattice spacings $d_{02.2}=1.406$ Å and $d_{03.0}=1.071$ Å were calculated. On the basis of these values the lattice parameters of hexagonal unit cell of MnAs nanoclusters, $a=3.710\pm0.002$ and $c=5.812\pm0.007$ Å, were determined. These values are close to those reported in Ref. 18.

The crystal structure of the bulk MnAs is hexagonal of NiAs-type with lattice parameters $a=3.7187$ and $c=5.7024$ Å (e.g., Ref. [33]). Differences between these values and those determined for MnAs nanoclusters result from both the lattice mismatch between the lattice parameters of MnAs and GaAs and the large difference between the thermal expansion coefficients for these compounds. Due to these effects, the oriented hexagonal MnAs clusters are distorted with respect to unstrained bulk MnAs. This distortion creates the biaxial strain ($\varepsilon_{11}=\varepsilon_{22}$) in {00.1} planes and along the c-axis (ε_{33}) in ⟨00.1⟩ directions. The values of these strains are $\varepsilon_{11}=\varepsilon_{22}=-0.2\times10^{-2}$, and $\varepsilon_{33}=1.8\times10^{-2}$.

Table 1
Values of the lattice parameters $a_{\perp}$, a_{rel} and in-plane strain ε, for $Ga_{(1-x)}Mn_xAs$ layers before and after annealing. The in-plane lattice parameter $a_{\parallel}$ for all studied layers is the same as that of GaAs substrate: $a_{\parallel}=a_{GaAs}=5.6533$ Å. All lattice parameters in are given in Å and were calculated with an accuracy of 10^{-4} Å.

Sample $Ga_{1-x}Mn_xAs$	$a_{\perp as\text{-}grown}$	$a_{\perp 500\ ^\circ C}$	$a_{\perp 600\ ^\circ C}$	$a_{relax\ as\text{-}grown}$	$a_{relax\ 500\ ^\circ C}$	$a_{relax\ 600\ ^\circ C}$	$\varepsilon_{as\text{-}grown}\times10^{-4}$	$\varepsilon_{500\ ^\circ C}\times10^{-4}$	$\varepsilon_{600\ ^\circ C}\times10^{-4}$
$x=0.025$	5.6658	5.6500	5.6479	5.6596	5.6517	5.6506	−11.1	2.8	4.8
$x=0.04$	5.6732	5.6471	5.6493	5.6633	5.6502	5.6513	−17.7	5.5	3.5
$x=0.05$	5.6763	5.6439	5.6505	5.6648	5.6486	5.6519	−20.3	8.3	2.5
$x=0.063$	5.6857	5.6475	5.6501	5.6695	5.6504	5.6517	−28.6	5.13	2.8

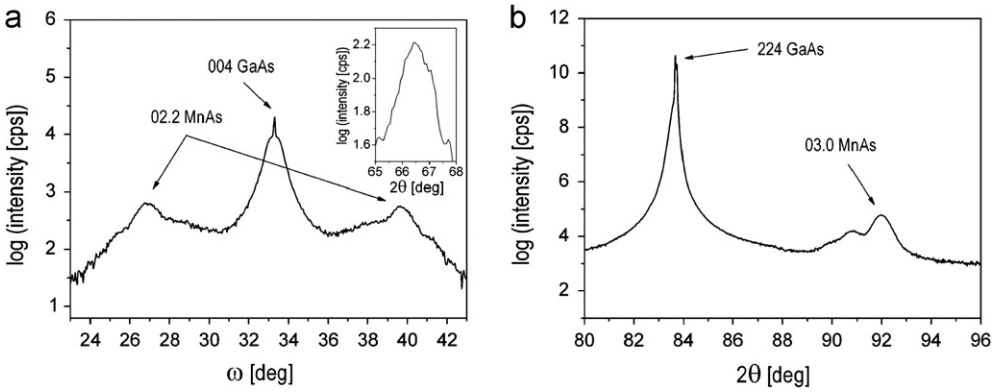

Fig. 5. The X-ray patterns for GaAs:Mn sample with $x=0.05$ after annealing at 600 °C. The ω scan around 004 GaAs reflection—(a) the inset displays the $2\theta/\omega$ scan of 02.2 reflection and (b) $2\theta/\omega$ scan in the vicinity of 224 GaAs reflection.

This means that the lattice parameter a of nanoclusters is compressed by only 0.20%, while the lattice parameter c is increased by 1.8%. Knowing the strains of the nanoclusters we can estimate the related stresses, δ_a and δ_c, through Hooke's law using the elastic constants for hexagonal MnAs [34]. The stresses δ_a and δ_c, along the a- and c-axes, respectively, are $\delta_a=-0.04$ GPa and $\delta_c=1.92$ GPa. The same stresses, δ_a and δ_c, but with opposite sign, act in the $\langle 110\rangle$ and $\langle 111\rangle$ directions of the matrix unit cell, decreasing its lattice parameter. The stress δ_a is very small compared with that acting in the $\langle 111\rangle$ direction, δ_c; therefore in further considerations we will take into account only $\delta_c=-1.92$ GPa. From this value of stress, using the bulk modulus (76 GPa) for GaAs [35] and pressure $p=1.92$ GPa, the lattice parameter of the hydrostatically compressed GaAs unit cell $a_{strained}=5.6057$ Å was determined. However, this value is much smaller than the experimental values, a_{rel}, obtained from our measurements for all investigated samples (see Table 1). Because the X-ray measurements give an average value of the lattice parameters of strained and unstrained unit cells, we can conclude that only part of the matrix unit cells is strained by hexagonal MnAs inclusions. The fraction of the strained unit cells (y) can be estimated from the simple equation:

$$y\,a_{GaAs\ strained}+(1-y)a_{GaAs}=a_{average}, \tag{3}$$

where $a_{average}$ is the relaxed lattice parameter (a_{rel}) obtained from measurement of the $Ga_{1-x}Mn_xAs$ layer after annealing and a_{GaAs} is the lattice parameter of unstrained GaAs unit cells.

In particular, for the $Ga_{0.95}Mn_{0.05}As$ layer annealed at 600 °C ($a_{rel}=5.6519$ Å), the fraction of the strained unit cells inside the GaAs matrix is $y=0.03$. This estimation was derived assuming the existence of only hexagonal MnAs inclusions, although according to other studies (TEM, EXAFS) nanoclusters of cubic GaMnAs are also created. The lattice parameter reported for cubic MnAs is ~5.9 Å (e.g., Ref. [30]). Unfortunately, the size of these inclusions is too small for detection by X-ray diffraction. As was shown in TEM studies, the creation of the clusters starts from the metastable, cubic small nanoclusters, which grow epitaxially on {111} GaAs planes. Calculation of the stress developed in the GaAs matrix by cubic (Ga,Mn)As nanoinclusions, using the above described method is impossible, because neither the strain state nor the elastic constant of cubic GaMnAs is known.

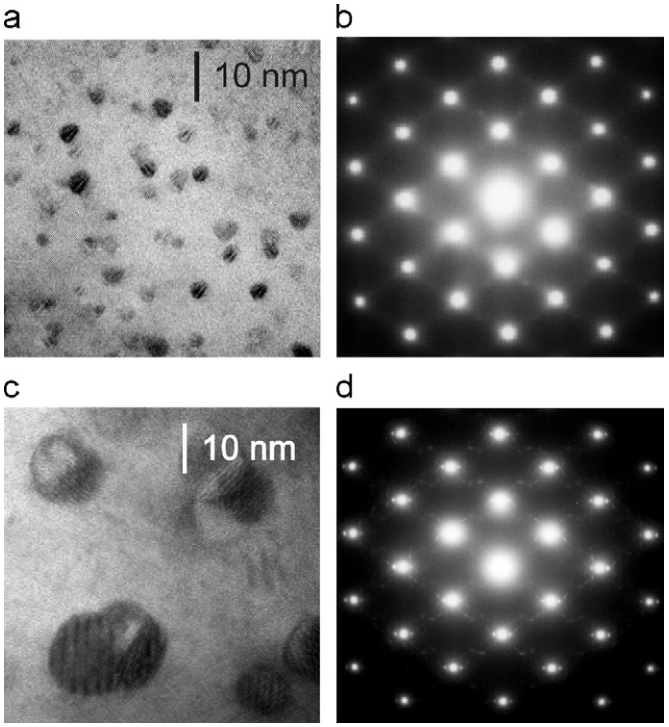

Fig. 6. Cross-sectional bright-field TEM images and electron diffraction patterns of granular GaAs:Mn layers obtained after annealing of $Ga_{1-x}Mn_xAs$ with two different Mn compositions x at 600 °C: (a),(b)—$x=0.025$, and (c),(d)—$x=0.063$.

3.3. Transmission electron microscopy studies

For all the annealed samples, nanoclusters were observed. Fig. 6 shows as an example cross-sectional TEM images of granular layers for samples with $x=0.025$ and $x=0.063$ annealed at 600 °C. It was

found that small clusters of sizes less than 10 nm have cubic ZB structure in contrast to the large nanoclusters, which have NiAs-type hexagonal structure. In both cases most of nanoclusters were coherently aligned with the GaAs matrix (Fig. 6b and d).

The Bragg spots from GaAs structure were visible on all the diffraction patterns. For $x=0.025$ (Fig. 6b) lines of weak diffuse intensities along $\langle 111 \rangle$ directions were present. These originated from nucleation of (Ga,Mn)As cubic clusters on the {111} planes of the GaAs matrix. On the diffraction pattern for the sample with $x=0.063$ (Fig. 6d) in addition to the spots from GaAs matrix week spots attributed to hexagonal MnAs clusters were visible. From the analysis of electron diffraction patterns it was found that the additional spots originated from NiAs-type hexagonal nanocrystals with {00.1} lattice planes parallel to the {111} of GaAs matrix and with MnAs $\langle 11.0 \rangle$ directions collinear with $\langle 110 \rangle$ of GaAs.

The distribution of nanocluster diameters is presented in Fig. 7. For the sample with the lowest Mn concentration ($x=0.025$), after annealing at 500 and 600 °C only small nanoclusters with diameter about 3–6 nm were found. For the sample with $x=0.05$ most of the nanoclusters have diameter between 6 and 11 nm already after annealing at 500 °C. After annealing at 600 °C only a few nanoclusters with diameter smaller than 10 remain; most of the nanoclusters have larger diameters. In the case of the sample with $x=0.063$, after annealing at 500 °C, only a small number of nanoclusters with diameter larger than 10 nm was found, and even after annealing at 600 °C a relatively large number of nanoclusters with small diameter were still detected.

The XRD results were compared with those obtained by TEM measurements. For the sample with the lowest Mn concentration $x=0.025$ no precipitations were detected by XRD, but the TEM image (Figs. 6a and b and 7) clearly shows the cubic nanoclusters with dominating diameters of about 3–6 nm. Simultaneously, after annealing at 600 °C the increase of the layer strain was detected by XRD (Table 1). This increase can be related to the further ordering of Mn in the cubic clusters. The opposite effect was observed for the layers with larger Mn concentrations ($x=0.05$ and 0.063): here annealing at higher temperature leads to creation of hexagonal MnAs clusters (see Fig. 6c and d and 7), which results in a decrease of the strain state of the layers (Table 1). However, the observed decrease of the layer strain was less pronounced for the sample with $x=0.063$, which can be connected to the presence of relatively large number of cubic nanoclusters in this sample as compared to the sample with $x=0.05$ (see Fig. 7).

The careful analysis of XRD and TEM results leads to the conclusion that the cubic inclusions exert higher stress on the matrix unit cells than the hexagonal ones.

3.4. X-ray absorption studies

The XRD and TEM measurements provide information about the crystallographic structure of the matrix and formed nanoclusters

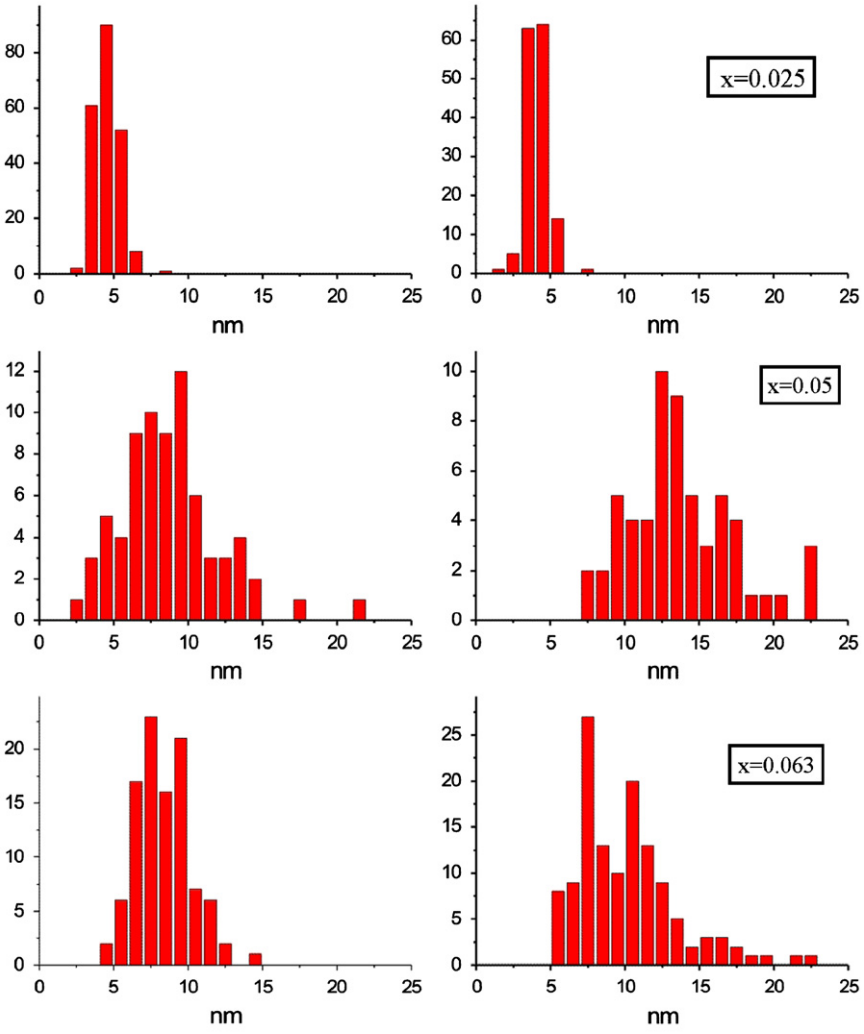

Fig. 7. Histograms of GaAs:Mn samples with $x=0.025$, $x=0.05$ and $x=0.063$ annealed at 500 °C (left column) and 600 °C (right column).

but do not allow to estimate the fraction of Mn atoms located in each kind of nanoclusters or their chemical composition. XAS probes the local atomic order around the absorbing atom; therefore, it is an ideal tool for the determination of the Mn location in the investigated structures [30,36–38]. The XAS spectra were analyzed using the IFEFFIT package [39]. The applied mathematical formalism represents a Real-Space Multiple-Scattering (RSMS) with summation of contributions from all single scattering paths of inner photoelectrons emitted during the absorption process.

In the analysis of the EXAFS spectra Mn based nanoclusters with ZB- and NiAs-type hexagonal structures immersed in the GaAs matrix were considered. Different values of lattice constants for hypothetical zinc-blende MnAs have been reported in the literature, namely 5.7, 5.9 and 5.98 Å [40–43]. Corresponding Mn–As bond lengths are ~2.47, ~2.55 and ~2.59 Å. In a starting model it was assumed that the distance of the first coordination sphere is equal to 2.55 Å and this distance was refined during the analysis, therefore this choice has no influence on the results of analysis. For the hexagonal inclusions, the NiAs-type structure ($P6_3/mmc$ space group) with the lattice constants $a=3.7187$ and $c=5.7024$ Å [33] was considered.

The amplitude-dumping factor (S_0^2), which is strongly correlated with coordination number N and disorder parameter sigma^2, was estimated similarly as in Ref. [30] and found to be 0.85; this value was used in all fittings. The data were analyzed from k_{min} around 2 Å^{-1} to k_{max} from 12.8 to 14.5 Å^{-1} depending on data quality. The fitting was performed in R space. The data were weighted by k^3 to enhance the oscillations for high k.

To keep the number of fitting parameters as small as possible, the parameter weighting the number of atoms in the coordination spheres according to the fraction of Mn atoms in each kind of nanoclusters was introduced. N1 represents the fraction (in %) of the Mn atoms bonded in nanoclusters with the cubic structure. The fraction of the Mn atoms bonded in nanoclusters with the hexagonal structure was assumed to be 100 − N1.

Taking into consideration the existence of hypothetical zinc blende MnAs, widely discussed in the literature, we have constructed a model of such structure. According to the atomic order in this structure, Mn atoms should have 4 As atoms as the nearest neighbors, in the second shell 12 Mn and next 12 As atoms. Surprisingly, while assuming the ZB order the Mn atoms cannot be found in the second coordination sphere for any of the investigated samples. Only Ga atoms in the second sphere provided physical parameters of the fit. We have also considered the possibility of the coexistence of GaMnAs solid solution and cubic MnAs nanoclusters. In all samples the fraction of MnAs ZB was at the detection limit. The amplitude and phase of the scattering photoelectrons remarkably differ for Mn and Ga atoms and can be easily distinguished during EXAFS analysis. To the authors' knowledge in none of the reported literature of EXAFS results, the existence of cubic inclusions with 12 Mn in the second shell was reported (see [30] and reference therein). Therefore, we can rule out the existence of hypothetic pure MnAs nanoclusters in the investigated samples. Only nanoclusters of (Ga,Mn)As zinc blende solid solution were found. The presence of one Mn atom in the second shell cannot be excluded because is at the level of the error in the EXAFS analysis. This gives in a 6 nm cluster the Mn concentration close to 20% [29]. The atomic distances and disorder parameters differ in ZB nanoclusters and depend on the Mn content and annealing temperature (see Tables 2 and 3). In average distances of the first As shell are systematically longer in samples annealed at 600 °C than in those annealed at 500 °C. The change of the inter-atomic distances can explain the variety of lattice parameters reported in the literature for hypothetic ZB MnAs and can be related to the stress induced into the matrix as was discussed in the XRD and TEM studies above.

In the case of the hexagonal structure, the distances and the coordination numbers N between the central atom and specific shells were kept according to crystallographic data. The sigma^2 parameters were fitted for all samples taking into account the fact that chemical disorder in clusters can differ from sample to sample. The numerical results of such fitting are collected in Table 2 for samples annealed at 500 °C and in Table 3 for samples annealed at 600 °C. The fractions of Mn atoms found in each phase are summarized in Table 4. The experimental data together with fitted models for the investigated samples are shown in Figs. 8–11.

Examining the parameters of the fitting procedures collected in Tables 2 and 3, one may notice that for ZB clusters the disorder parameter sigma^2 is rather high for the second and third spheres. This is obviously related to the small dimension of these clusters and scatter of the Mn content. In the case of hexagonal nanoclusters the relatively high disorder was found in the forth sphere composed of As atoms with the distance close to As atoms in ZB clusters. Therefore, the inter-path correlations stress on the sigma^2 parameters and lead to the increase of the estimated error of given parameter.

Considering the existence of both kind of clusters one should notice that they differ already in the first coordination shell (4 As atoms in ZB structure and 6 As in hexagonal structure of MnAs). Therefore, the proportion between these two kinds of cluster can be estimated already from consideration of only first shell. Nevertheless, we were able to get good fit considering all shells up to 4.8 Å. Neglecting the existence of two kinds of clusters

Table 2

The inter-atomic distances R (Å) in the subsequent coordination spheres, and disorder parameters sigma^2 (Å^2) as estimated for samples after annealing at 500 °C. *Rf* denotes the parameter describing the quality of fitting, N1 the fraction of nanocluster in zinc blende structure.

Atom (# in the shell)	R (Å)	Sigma^2 (Å^2)	R (Å)	Sigma^2 (Å^2)	R (Å)	Sigma^2 (Å^2)	R (Å)	Sigma^2 (Å^2)
Sample	$x=0.025$ *Rf*=0.0005		$x=0.04$ *Rf*=0.0001		$x=0.05$ *Rf*=0.0003		$x=0.063$ *Rf*=0.0002	
*N*1 (%)	100		72(2)		53(5)		69(2)	
As (4)	2.557(2)	0.0055(6)	2.52(1)	0.008(1)	2.55(1)	0.005(1)	2.53(1)	0.006(1)
Ga (12)	4.06(4)	0.025(6)	4.15(7)	0.034(8)	4.07(4)	0.013(5)	4.10(4)	0.024(5)
As (12)	4.73(3)	0.018(4)	4.49(6)	0.029(7)	4.27(5)	0.011(4)	4.48(3)	0.018(3)
100 − *N*1 (%)	0		28		47		31	
As (6)			2.58	0.003(2)	2.58	0.006(1)	2.58	0.002(1)
Mn (2)			2.85	0.02(1)	2.85	0.005(3)	2.85	0.005(4)
Mn (6)			3.72	0.015(8)	3.72	0.013(9)	3.72	0.006(5)
As (6)			4.52	0.013(9)	4.52	0.011(6)	4.52	0.02(1)
Mn (12)			4.69	0.002(1)	4.69	0.011(9)	4.69	0.004(1)
As (6)			4.79	0.0012(8)	4.79	0.007(4)	4.79	0.003(1)

Table 3
The inter-atomic distances R (Å) in the subsequent coordination spheres, and disorder parameters sigma^2 (Å^2) as estimated for samples after annealing at 600 °C. *Rf* denotes the parameter describing the quality of fitting; $N1$ the fraction of nanocluster in zinc blende structure.

Atoms (# in the shell) Sample	R (Å)	Sigma^2 (Å^2)	R (Å)	Sigma^2 (Å^2)	R (Å)	Sigma^2 (Å^2)	R (Å)	Sigma^2 (Å^2)
	x=0.025 *Rf*=0.0002		x=0.04 *Rf*=0.0001		x=0.05 *Rf*=0.0002		x=0.063 *Rf*=0.0003	
$N1$ (%)	100		40(5)		15(5)		50(5)	
As (4)	2.577(4)	0.0049(2)	2.54(1)	0.006(1)	2.55(1)	0.002(1)	2.57(1)	0.006(1)
Ga (12)	4.23(4)	0.025(7)	4.13(4)	0.012(6)	4.10(4)	0.006(4)	4.19(3)	0.017(4)
As (12)	4. 68(2)	0.017(3)	4.29(7)	0.014(8)	4.24(3)	0.005(3)	4.73(5)	0.02(1)
100−$N1$ (%)	0		60		85		50	
As (6)			2.58	0.005(1)	2.58	0.0047(2)	2.58	0.004(1)
Mn (2)			2.85	0.010(4)	2.85	0.007(3)	2.85	0.005(2)
Mn (6)			3.72	0.017(5)	3.72	0.011(3)	3.72	0.010(3)
As (6)			4.52	0.026(9)	4.52	0.012(4)	4.52	0.026(9)
Mn (12)			4.69	0.0010(3)	4.69	0.009(3)	4.69	0.009(3)
As (6)			4.79	0.006(3)	4.79	0.006(2)	4.79	0.005(3)

Table 4
The percentage of Mn atoms in (Ga,Mn)As ZB clusters and in hexagonal MnAs clusters as estimated by EXAFS analysis.

Sample	Annealed at 500 °C		Annealed at 600 °C	
Clusters	ZB (%)	Hexagonal (%)	ZB (%)	Hexagonal (%)
x=0.025	100	0	100	0
x=0.04	72(2)	28	40(5)	60
x=0.05	53(5)	47	15(5)	85
x=0.063	69 (2)	31	50(5)	50

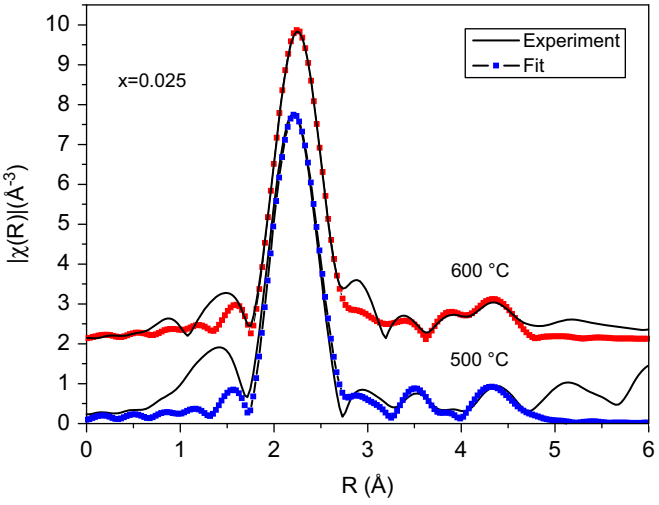

Fig. 8. GaAs:Mn with x=0.025 annealed at 500 °C and 600 °C. Model of (Ga,Mn)As ZB clusters with 12 Ga in second shell. Fourier transform of the EXAFS (full line) and the result of fitting (squares).

resulted with unphysical coordination number N in the first shell as is reported in some of EXAFS papers [44].

Let's analyze the data collected in Table 4 showing the fraction of Mn atoms in ZB (Ga,Mn)As and hexagonal MnAs nanoclusters together with the dimensions of clusters presented in Fig. 7. One can notice that for samples with small amounts of Mn, x=0.025 small clusters with ZB structure were detected. For the sample with x=0.05 annealed at 500 °C small clusters and those with dimensions up to 15 nm are seen, and from EXAFS analysis almost 50% of (Ga,Mn)As ZB and hexagonal inclusion have been obtained. After annealing at 600 °C most clusters have dimensions between

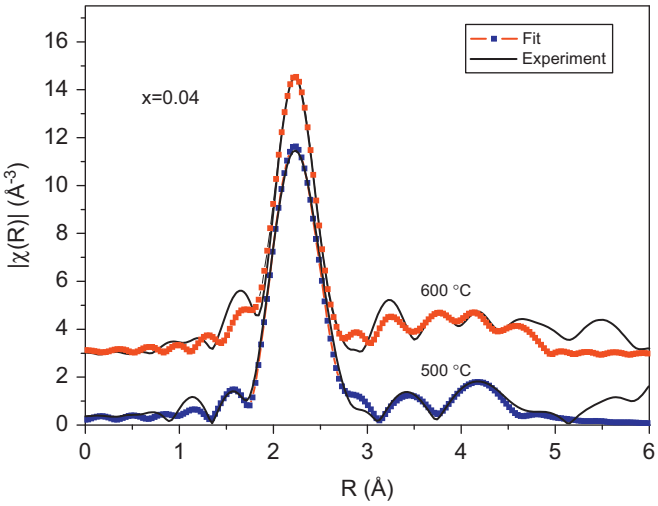

Fig. 9. GaAs:Mn with x=0.04 annealed at 500 and 600 °C. Model of 72% (Ga,Mn)As ZB and 28% MnAs hexagonal clusters for 500 °C and model of 40% (Ga,Mn)As ZB and 60% of MnAs hexagonal clusters for 600 °C. Fourier transform of the EXAFS (full line) and the result of fitting (squares).

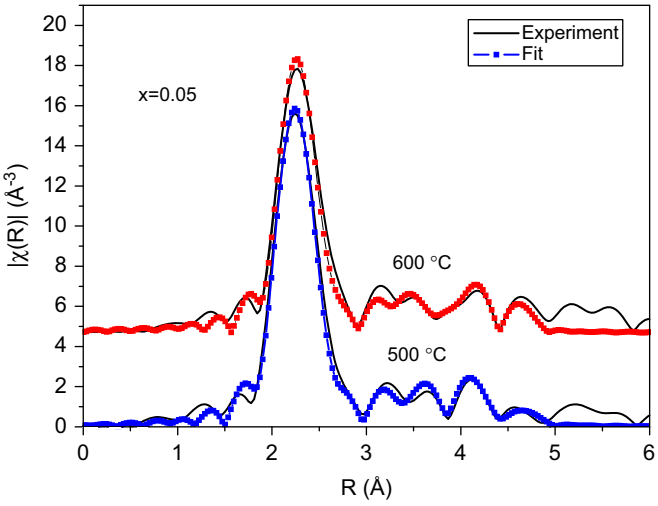

Fig. 10. GaAs:Mn with x=0.05 annealed at 500 and 600 °C. Model of 53% (Ga,Mn)As ZB and 47% MnAs hexagonal clusters for 500 °C and model of 15% (Ga,Mn)As ZB and 85% of MnAs hexagonal clusters for 600 °C. Fourier transform of the EXAFS (full line) and the result of fitting (squares).

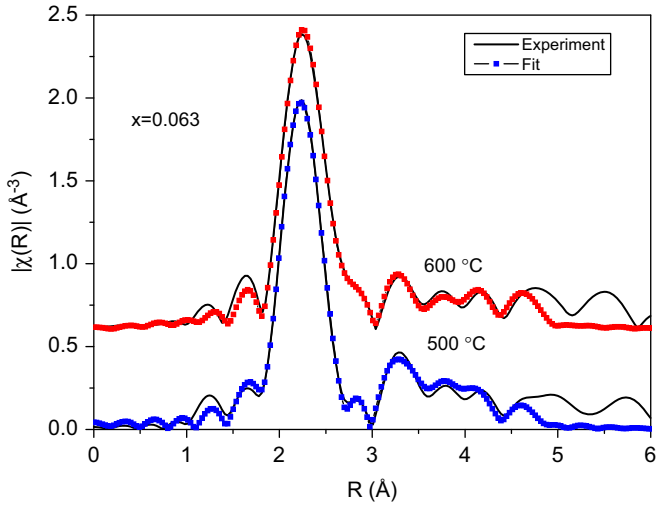

Fig. 11. GaAs:Mn with $x=0.063$ annealed at 500 and 600 °C. Model of 69% (Ga,Mn)As ZB and 31% MnAs hexagonal clusters for 500 °C and model of 50% (Ga,Mn)As ZB and 50% of MnAs hexagonal clusters for 600 °C. Fourier transform of the EXAFS (full line) and the result of fitting (squares).

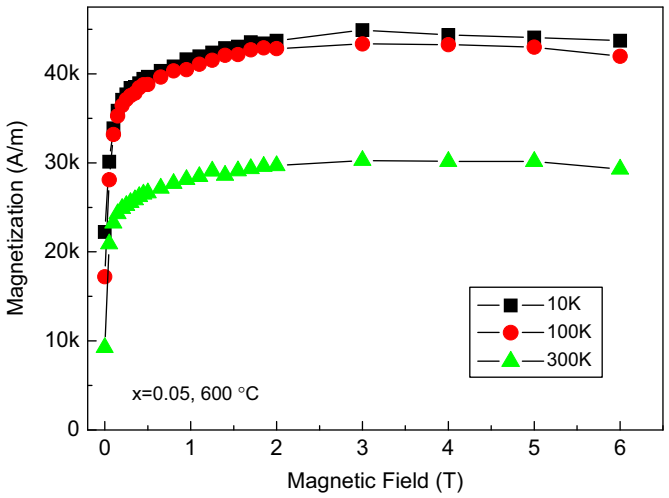

Fig. 12. Magnetization of sample with $x=0.05$ annealed at 600 °C as a function of magnetic field measured at 10, 100 and 300 K.

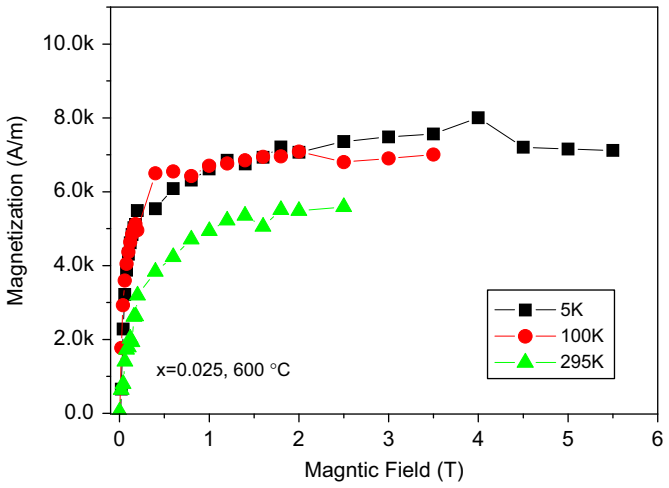

Fig. 13. Magnetization of sample with $x=0.025$ annealed at 600 °C as a function of magnetic field measured at 5, 100 and 295 K.

10 and 20 nm and EXAFS found only 15% of ZB clusters. In the case of the sample with $x=0.063$ after annealing at 500 °C the histogram shows that most clusters have dimensions between 5 and 10 nm, and EXAFS found 69% of Mn atoms in (Ga,Mn)As ZB clusters. For the sample annealed at 600 °C still almost 50% small clusters were seen, and EXAFS detected 50% of Mn atoms in (Ga,Mn)As ZB clusters. Therefore, our studies performed by TEM and EXAFS are in agreement with the statement reported in many papers, that small clusters (here up to 6–8 nm) in GaAs matrix have ZB structure and larger ones—hexagonal structure. Moreover, the annealing at 600 °C is not sufficient to convert all clusters into hexagonal inclusions. In Ref. [37] the EXAFS studies of the as-grown samples from the same series have been presented and the fractions of Mn in the substitutional and interstitial position estimated. Only in the sample with $x=0.025$, 90% of Mn atoms were located in the Ga position. In all other samples more than 40% of Mn atoms were in the interstitial position. After annealing of the sample with $x=0.025$, only ZB inclusions were formed. In the case of other samples, annealing at 500 °C was sufficient to form some hexagonal inclusions. It may imply that Mn in Ga position is more difficult to convert into hexagonal inclusions even by annealing at 600 °C, but Mn in interstitial position easily forms hexagonal inclusions already during 500 °C annealing. The Mn–As bond length in the substitutional position in as-grown samples was found to be 2.48 Å. The Mn–As bond in the ZB nanoclusters is longer ~2.55 Å and leads to tensile strain of the layer as was observed in XRD studies.

3.5. Magnetic studies

In order to get more information about the clusters properties the structural study was supplemented by magnetization measurements. As it was mentioned in the introduction both hexagonal MnAs and cubic GaMnAs are ferromagnets; however, critical temperature of MnAs is about 320 K, while for the GaMnAs it varies with Mn concentration and hardly reaches 190 K [15]. Therefore above 200 K GaMnAs behaves as a paramagnet, while hexagonal MnAs is still in a ferromagnetic state.

The magnetic behavior of our composite is illustrated in Figs. 12 and 13, where magnetization of the samples with $x=0.05$ (Fig. 12) annealed at 600 °C and, $x=0.025$ (Fig.13) annealed at 600 °C is plotted as a function of magnetic field for several temperatures.

In the case of the sample containing both hexagonal MnAs and cubic (Ga,Mn)As inclusions as discussed above ($x=0.05$, Fig. 12) magnetization shows typical ferromagnetic-like behavior (i.e. very fast saturation with magnetic field) even at 300 K, in agreement with magnetic properties of bulk MnAs. Similar fast saturation of magnetization with magnetic field is also observed for the sample containing solely cubic (Ga,Mn)As inclusions ($x=0.025$, Fig. 13). While it is not surprising at low temperatures, where inclusions built of ferromagnetic GaMnAs may reveal such behavior, very fast magnetizing of the system at 295 K, where bulk GaMnAs is paramagnetic, is not expected. As it was discussed recently [29] this may suggest that these clusters are formed of GaMnAs with Mn concentrations higher than 15% (the highest in the GaMnAs epilayers in substitutional position), yet still well below 100% (MnAs). Monte Carlo simulations for GaMnAs layers with increasing content of Mn showed that Curie temperature reaches room temperature for content of Mn close to 20%. On the other hand, with decrease in temperature increase in saturation magnetization may result from Mn concentration dispersion over different inclusions. At low temperatures (below 100 K) all inclusions are ferromagnetic, whereas at high temperatures (e.g. ambient temperature) the cubic inclusions with x smaller than roughly 20% are paramagnetic and their contribution

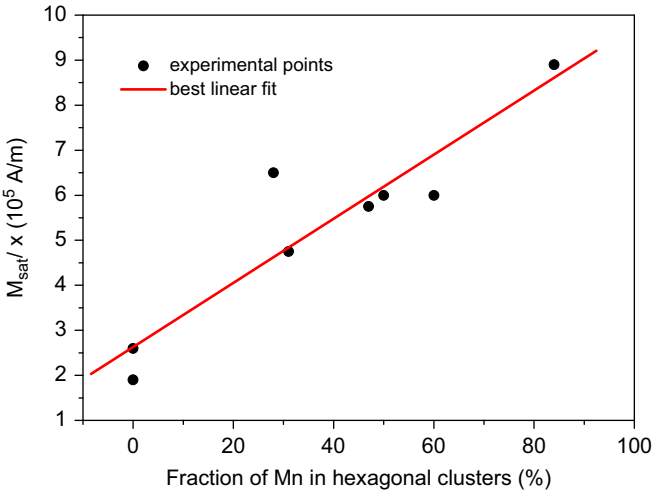

Fig. 14. Saturated magnetization per unit composition evaluated at $T=10$ K versus fraction of Mn in hexagonal MnAs clusters.

to magnetization at moderate fields (below 5 T) is negligible. Thus the total magnetization saturates at values lower than those at low temperatures.

The difference between hexagonal MnAs and cubic (Ga,Mn)As clusters is exemplified in Fig.14, where saturated magnetization per unit composition M/x (evaluated at $T=10$ K) versus the fraction of hexagonal clusters is plotted. Apparently magnetic moment per Mn ion is higher at hexagonal MnAs clusters than in cubic clusters (Ga,Mn)As. For the samples where both hexagonal MnAs and cubic (Ga,Mn)As clusters are present saturated magnetization should be the average of the extreme values, which seems to be the case (Fig. 14).

Details of the magnetic study of our samples will be published elsewhere. We only mention here that the possibility to have clusters, which are ferromagnetic at room temperature, is very promising for spintronic applications.

4. Conclusions

The set of $Ga_{1-x}Mn_xAs$ layers grown on GaAs (001) substrate with different contents of Mn and annealed at 500 or 600 °C was studied. For samples annealed at lower temperatures, creation of predominantly cubic nanoclusters was observed. In the case of layers with small Mn concentration annealed at higher temperatures, formation of only cubic nanoclusters was still detected. However, for the samples with higher Mn concentration, already at 500 °C hexagonal inclusions were formed, and annealing at 600 °C led to creation of a higher number of hexagonal nanoinclusions. Therefore, a priori assumption of a given type of clusters formation is not justified. The tensile strain of the GaAs matrix related to the creation of Mn-containing cubic nanoclusters was larger than for hexagonal ones, which indicates that cubic inclusions act with larger stress on the matrix unit cells than the hexagonal nanoinclusions. This explain the different lattice constants of annealed GaMnAs layers as observed in XRD studies.

XAFS studies rule out the possibility of the formation of a hypothetic MnAs ZB compound, widely discussed in the literature. Only (Ga,Mn)As ZB clusters were detected. In all samples, in order to get reasonable fit of EXAFS data to the model, the Ga atoms have to be located in the second coordination sphere around Mn atoms instead of Mn as in MnAs ZB. The comparison of the distribution of nanocluster dimensions estimated from TEM with the fraction of Mn atoms found by EXAFS in (Ga,Mn)As ZB and the hexagonal MnAs clusters were in agreement with the fact that clusters up to 6–8 nm have ZB structure and larger ones—the hexagonal structure. The fraction of Mn found in hexagonal structure was directly related to magnetic properties of samples. Moreover, the ZB clusters found in the sample containing solely the cubic (Ga,Mn)As clusters remain ferromagnetic even at room temperature. According to the recent calculations [29] this fact implies that the content of Mn in these (Ga,Mn)As ZB clusters should be close to 20%. Saturation magnetization divided by Mn content indicated on a bimodal distribution of Mn magnetic moments, higher for hexagonal clusters and lower for (Ga,Mn)As ZB clusters.

Acknowledgments

This work was partially supported by a national grant of Ministry of Science and High Education N202-052-32/1189. The measurements performed at synchrotron have received funding from the European Community's Seventh Framework Program (FP7/2007-2013) under grant agreement no. 226716.

References

[1] H. Ohno, A. Shen, F. Matsukura, A. Oiwa, A. Endo, S. Katsumoto, Y. Iye, Appl. Phys. Lett. 69 (1996) 363–365.
[2] T. Dietl, H. Ohno, F. Matsukura, J. Cibert, D. Ferrand, Science 287 (2000) 1019–1022.
[3] T. Dietl, F. Matsukura, H. Ohno, Phys. Rev. B 66 (2002) 033203-1–4.
[4] T. Jungwirth, J. Sinova, J. Masek, J. Kucera, A.H. MacDonald, Rev. Mod. Phys. 78 (2006) 809–864.
[5] S. Lee, D.Y. Shin, S.J. Chung, X. Liu, J.K. Furdyna, Appl. Phys. Lett. 90 (2007) 152113-1–3.
[6] Y. Mizuno, S. Ohya, P.N. Hai, M. Tanaka, Appl. Phys. Lett. 90 (2007) 162505-1–3.
[7] M. Ciorga, M. Schlapps, A. Einwanger, S. Geißler, J. Sadowski, W. Wegscheider, D. Weiss, New J. Phys. 9 (351) (2007) 1–17.
[8] Y. Nishitani, D. Chiba, F. Matsukura, H. Ohno, J. Appl. Phys 103 (2008) 07D139-1–3.
[9] D. Chiba, Y. Nishitani, F. Matsukura, H. Ohno, Appl. Phys. Lett. 90 (2007) 122503-1–3.
[10] S. Mack, R.C. Myers, J.T. Heron, A.C. Gossard, D.D. Awschalom, Appl. Phys. Lett. 92 (2008) 192502-1–3.
[11] K.W. Edmonds, P. Boguslawski, K.Y. Wang, R.P. Campion, N. Novikov, N.R.S. Farley, B.L. Gallagher, C.T. Foxon, M. Sawicki, T. Dietl, M. Buongiorno Nardelli, J. Bernholc, Phys. Rev. Lett. 92 (2004) 037201-1–4.
[12] B.J. Kirby, J.A. Borchers, J.J. Rhyne, S.G.E. Velthuis, A. Hoffmann, K.V. O'Donovan, T. Wojtowicz, X. Liu, W.L. Lim, J.K. Furdyna, Phys. Rev. B 69 (2004) 081307-1–4.
[13] M. Adell, L. Ilver, J. Kanski, V. Stanciu, P. Svedlindh, J. Sadowski, J.Z. Domagala, F. Terki, C. Hernandez, S. Charar, Appl. Phys. Lett. 86 (2005) 112501-1–3.
[14] K.M. Yu, W. Walukiewicz, T. Wojtowicz, I. Kuryliszyn, X. Liu, Y. Saaki Y, J.K. Furdyna, Phys. Rev. B 65 (2002) 201303-1–4.
[15] L. Chen, S. Yan, P.F. Xu, J. Lu, W.Z. Wang, J.J. Deng, X. Qian, Y. Ji, J.H. Zhao, Appl. Phys. Lett. 95 (2009) 182505-1–3.
[16] M. Moreno, A. Trampert, B. Jenichen, L. Däweritz, K.H. Ploog, J. Appl. Phys. 92 (2002) 4672–4677.
[17] M. Moreno, B. Jenichen, V.M. Kaganer, W. Braun, L.A. Trampert, L. Däweritz, K.H. Ploog, Phys. Rev. B 67 (2003) 235206-1–8.
[18] M. Moreno, V.M. Kaganer, B. Jenichen, A. Trampert, L. Däweritz, K.H. Ploog, Phys. Rev. B 72 (2005) 115206-1–8.
[19] M. Moreno, B. Jenichen, L. Däweritz, K.H. Ploog, Appl. Phys. Lett. 86 (2005) 161903-1–3.
[20] M. Yokoyama, H. Yamaguchi, T. Ogawa, M. Tanaka, J. Appl. Phys 97 (2005) 10D317-1–3.
[21] A. Kwiatkowski, D. Wasik, M. Kaminska, R. Bozek, J. Szczytko, A. Twardowski, J. Borysiuk, J. Sadowski, J. Gosk, J. Appl. Phys. 101 (2007) 113912-1–6.
[22] O.D.D. Couto, M.J.S.P. Brasil, F. Iikawa, C. Giles, C. Adriano, J.R.R. Bortoleto, M.A.A. Pudenzi, H.R. Gutierrez, I. Danilov, Appl. Phys.Lett. 86 (2005) 071906-1–3.
[23] M. Jamet, A. Barski, T. Devillers, V. Poydenot, R. Dujardin, P. Bayle-Guillemaud, J. Rothman, E. Bellet-Amalric, A. Marty, J. Cibert, R. Mattana, S. Tatarenko, Nat. Mater. 5 (2006) 653–659.
[24] S. Kuroda, N. Nishizawa, K. Takita, M. Mitome, Y. Bando, K. Osuch, T. Dietl, Nat. Mater. 6 (2007) 440–446.
[25] T. Dietl, J. Appl. Phys 103 (2008) 07D111-1–6.
[26] M. Rovezzi, F. D'Acapito, A. Navarro-Quezada, B. Faina, T. Li, A. Bonanni, F. Filippone, A.A. Bonapasta, T. Dietl, Phys. Rev. B 79 (2009) 195209-1–9.
[27] P.N. Hai, S. Ohya, M. Tanaka, S.E. Barnes, S. Maekawa, Nature 458 (2009) 489–492.

[28] M. Moreno, J.I. Cerdá, K.H. Ploog, K. Horn, Phys. Rev. B 82 (2010) 045117.
[29] K. Lawniczak-Jablonska, J. Libera, A. Wolska, M.T. Klepka, P. Dluzewski, J. Sadowski, D. Wasik, A. Twardowski, A. Kwiatkowski, K. Sato, Phys. Status Solidi RRL 5 (2011) 62–64.
[30] I.N. Demchenko, K. Lawniczak-Jablonska, T. Story, V. Osinniy, R. Jakiela, J.Z. Domagala, J. Sadowski, M. Klepka, A. Wolska, M. Chernyshova, J. Phys.: Condens. Matter 19 (496205) (2007) 1–14.
[31] K.X. Zhao, C.R. Staddon, K.Y. Wang, K.W. Edmonds, R.P. Campion, B.L. Gallangher, C.T. Foxon, Appl. Phys. Lett. 86 (2005) 071902-1–3.
[32] J. Sadowski, J.Z. Domagala, J. Kanski, C.H. Rodriguez, F. Terki, S. Chabar, D. Maude, Mater. Sci.—Poland 24 (3) (2006) 617–626.
[33] J. Mira, F. Rivadulla, J. Rivas, A. Fondado, T. Guidi, R. Caciuffo, F. Carsughi, P.G. Radaelli, J.B. Goodenough, Phys. Rev. Lett. 90 (2003) 097203-1–4.
[34] M. Dörfer, K. Bärner, Phys. Status Solidi A 17 (1973) 141–148.
[35] H.J. McSkimin, A. Jayaraman, P. Andreatch Jr., J. Appl. Phys. 38 (1967) 2362–2364.
[36] R. Bacewicz, A. Twarog, A. Malinowska, T. Wojtowicz, X. Liu, J.K. Furdyna, J. Phys. Chem. Sol. 66 (2005) 2004–2007.
[37] K. Lawniczak-Jablonska, J. Libera, A. Wolska, M.T. Klepka, R. Jakiela, J. Sadowski, Rad. Phys. Chem. 78 (2009) S80–S85.
[38] A. Wolska, K. Lawniczak-Jablonska, M.T. Klepka, R. Jakiela, J. Sadowski, I.N. Demchenko, E. Holub-Krappe, A. Persson, D. Arvanitis, Acta Phys. Pol. 114 (2008) 357–366.
[39] B. Ravel, M. Newville, J. Synchrotron Rad. 12 (2005) 537–541.
[40] R. Shioda, K. Ando, T. Hayashi, M. Tanaka, Phys. Rev. B 58 (1998) 1100–1102.
[41] H.M. Hong, Y.J. Kang, J. Kang, E.C. Lee, Y.H. Kim, K.J. Chang, Phys. Rev. B 72 (2005) 144408-1–7.
[42] G.M. Schott, W. Faschinger, L.W. Molenkamp, Appl. Phys. Lett. 79 (2001) 1807–1809.
[43] Y.L. Soo, S.W. Huang, Z.H. Ming, Y.H. Kao, H. Munekata, L.L. Chang, Phys. Rev. B 53 (1996) 4905–4909.
[44] F. d'Acapito, G. Smolentsev, F. Boscherini, M. Piccin, G. Bais, S. Rubini, F. Martelli, A. Franciosi, Phys. Rev. B 73 (2006) 035314-1–6.